Supporting Information

Construction of Sb_2S_3@NC Core-Shell Nanorod with Hollow Feature as Anode via Microstructure Regulation Strategy for High-Performance Na^+/K^+ Storage

*Authors: Rong Jiang[a], Junyuan Huang[a], Ruixue Ma[a], Qian Li[a], Longjun Dai[a], Runyu Li[a], Xingpeng Chen[a], Yang Ren[a], Zhu Liu[a, b], Xu Chen[c], Xiaowei Zhou[a,] **

[a] Department of Physics, School of Physics and Astronomy, Yunnan University, Kunming, 650504, China.

[b] Yunnan Key Laboratory of Micro/Nano-Materials and Technology, School of Materials and Energy, Yunnan University, Kunming 650504, China

[c] Institute of Criminal Investigation, Yunnan Police College, Kunming 650504, China

* Corresponding author's e-mail: zhouxiaowei@ynu.edu.cn

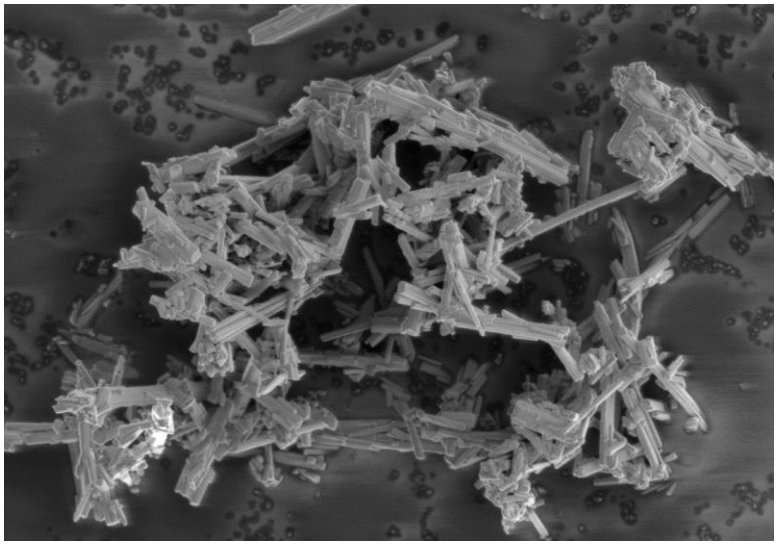

Fig.S1. SEM images of Sb_2S_3 NRs

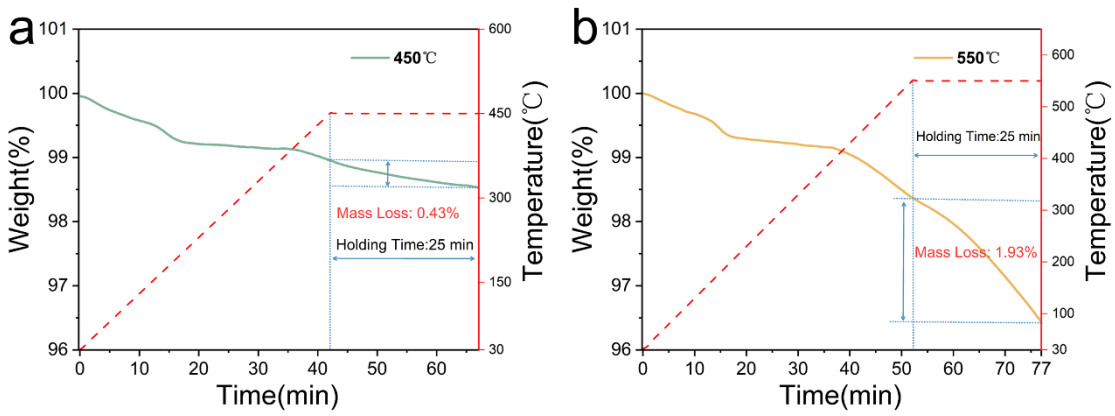

Fig.S2. TGA curves of commercial Sb powder measured at a heating rate of 10 °C/min: (a) heated to 450 °C and held for 25 min; (b) heated to 550 °C and held for 25 min.

For quantitative analysis of Sb_2S_3 volatilization, TGA was performed on commercial Sb_2S_3 powder at 450 °C and 550 °C separately. Under Ar atmosphere, the powder was heated to the target temperatures at a rate of 10 °C min^{-1} and held isothermally for 25 min, with volatilization rates at the two temperatures compared based on mass loss data. As shown in Fig.S2, after isothermal holding at 450 °C and 550 °C for 25 min, the sample exhibited mass losses of 0.43% and 1.93%, respectively. The volatilization rate at 550 °C was approximately 4.5 times that at 450 °C, demonstrating a notably higher volatilization rate of Sb_2S_3 at 550 °C.

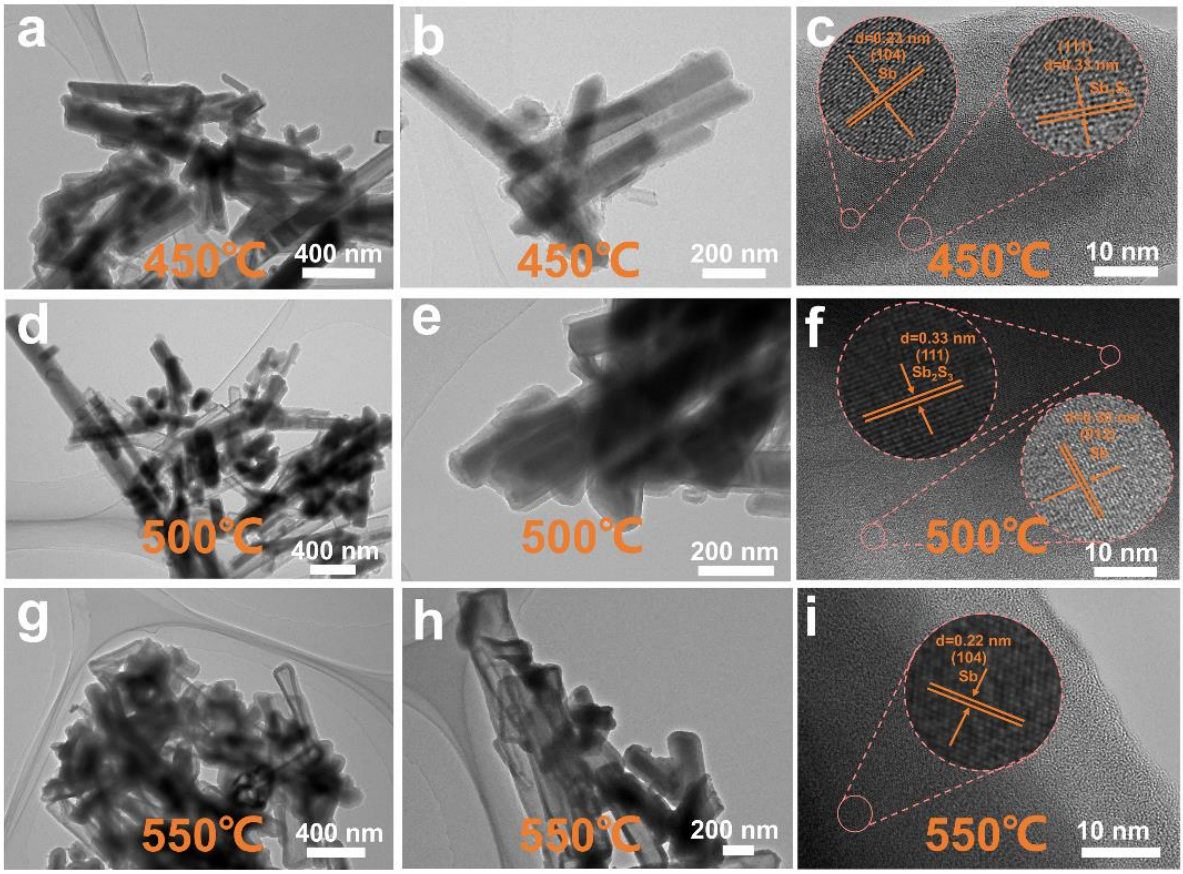

Fig.S3. TEM images of Sb_2S_3@PDA precursors calcined at various temperatures

TEM characterization was conducted on the intermediate products obtained at carbonization temperatures of 450, 500, and 550 °C, with the results presented in Fig.S3. Fig.S3 (a–c) show the TEM images of Sb_2S_3@PDA precursors after carbonization at 450 °C for 3 h, where no obvious void structures were observed within the NC layer; the interplanar spacings derived from HRTEM measurements correspond to the (104) crystal plane of Sb and the (111) crystal plane of Sb_2S_3, respectively. When the carbonization temperature was increased to 500 °C, the TEM images at different resolutions are displayed in Fig.S3 (d–f); at this temperature, no void structures were still detected in the NC layer, and the interplanar spacings characterized by HRTEM match well with the (012) crystal plane of Sb and the (111) crystal plane of Sb_2S_3, respectively. When the carbonization temperature was further elevated to 550 °C (Fig.S3 (g–i)), distinct pore structures appeared inside the NC layer,

and the corresponding interplanar spacings from HRTEM correspond to the (104) crystal plane of Sb.

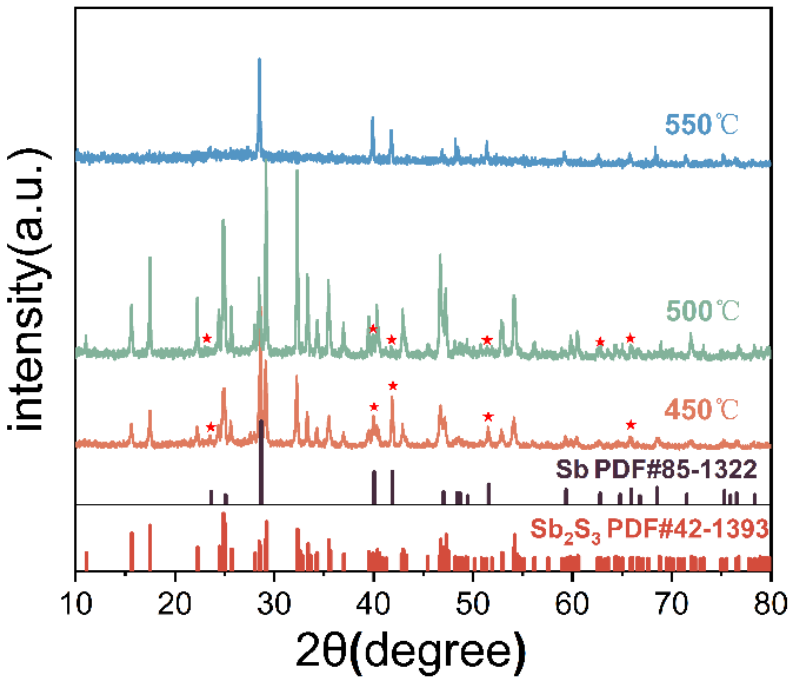

Fig.S4. XRD patterns of Sb_2S_3@PDA precursors calcined at various carbonization temperatures.

In addition, XRD characterization was performed on the three aforementioned intermediate products, with the results illustrated in Fig.S4. Both the samples obtained at 450°C and 500°C exhibited characteristic diffraction peaks corresponding to Sb_2S_3 and Sb, whereas only the characteristic diffraction peaks of Sb were detected for the sample prepared at 550°C. This finding is consistent with the conclusions derived from TEM characterization. These results demonstrate that a significant regulatory effect on the internal voids of the NC layer can only be achieved when the carbonization temperature is elevated to 550°C. This is because this temperature precisely reaches the melting point of Sb_2S_3, resulting in a higher volatilization rate than that at the other two temperatures; during high-temperature carbonization, partial Sb_2S_3 is volatilized, thereby forming distinct void structures inside the NC layer.

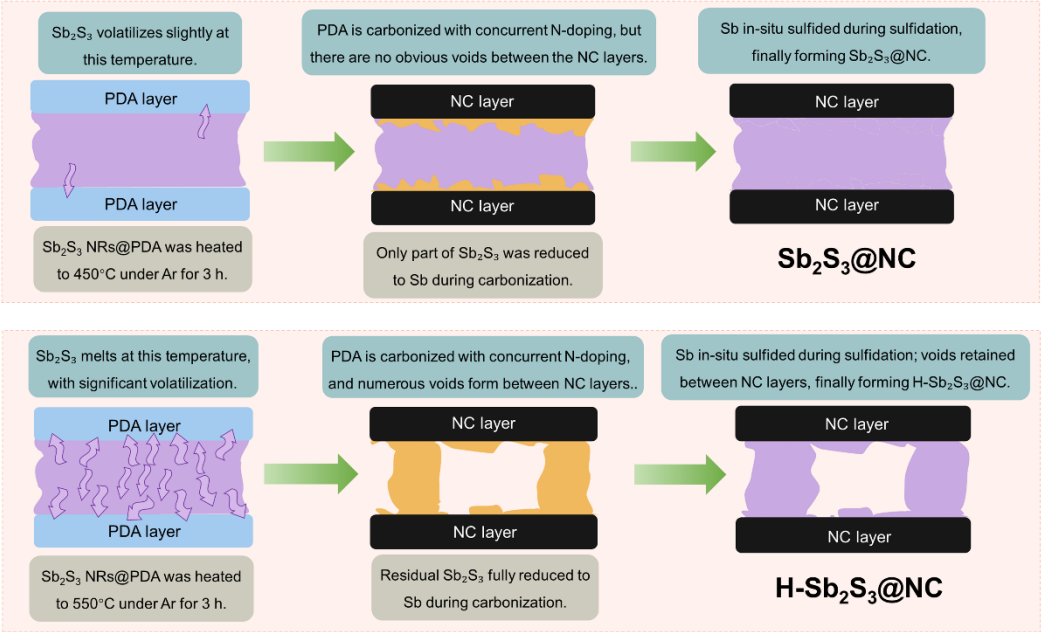

Fig.S5. Schematic Diagram of the Structure Formation Mechanism for Sb_2S_3@NC and H-Sb_2S_3@NC.

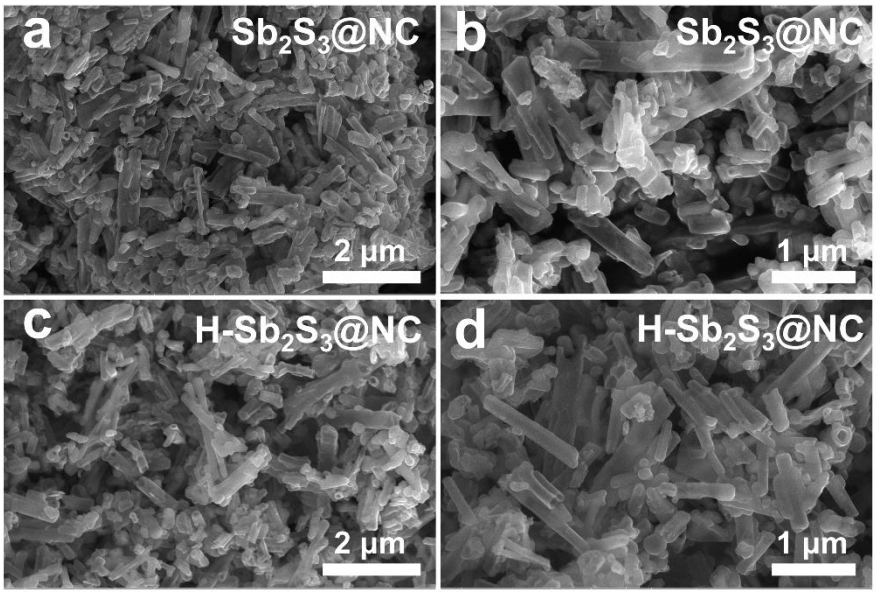

Fig.S6. SEM images of (a, b) Sb_2S_3@NC and (c, d) H-Sb_2S_3@NC at different magnifications.

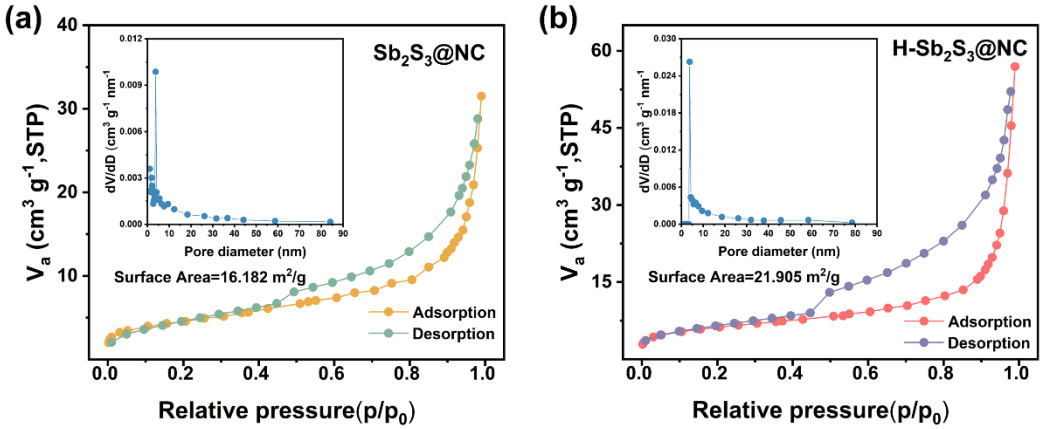

Fig.S7. (a,b) show the N_2 adsorption and desorption isotherms of the two samples, with the inset displaying the corresponding BJH pore size distribution.

The specific surface areas and pore size distributions of Sb_2S_3@NC and H-Sb_2S_3@NC were determined via N_2 adsorption-desorption measurements, as presented in Fig.S7. The specific surface areas of Sb_2S_3@NC and H-Sb_2S_3@NC were 16.182 and 21.905 $m^2\ g^{-1}$, with corresponding pore volumes of 0.048 and 0.084 $cm^3\ g^{-1}$, respectively. The larger specific surface area and pore volume of H-Sb_2S_3@NC further confirm that the volatilization of partial Sb_2S_3 in the Sb_2S_3@PDA precursor at 550 °C generates more void structures.

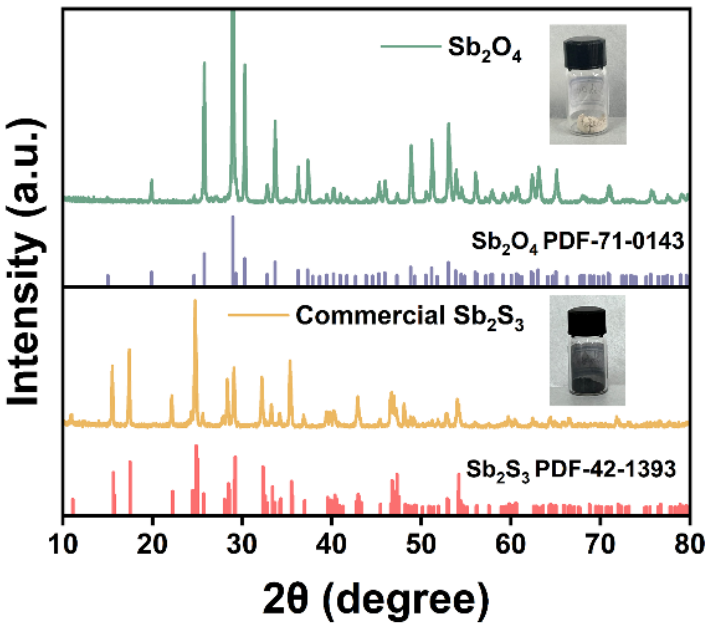

Fig.S8. XRD pattern of commercial Sb_2S_3 powder after heating to 800℃ at a heating rate of 10 ℃/min in air.

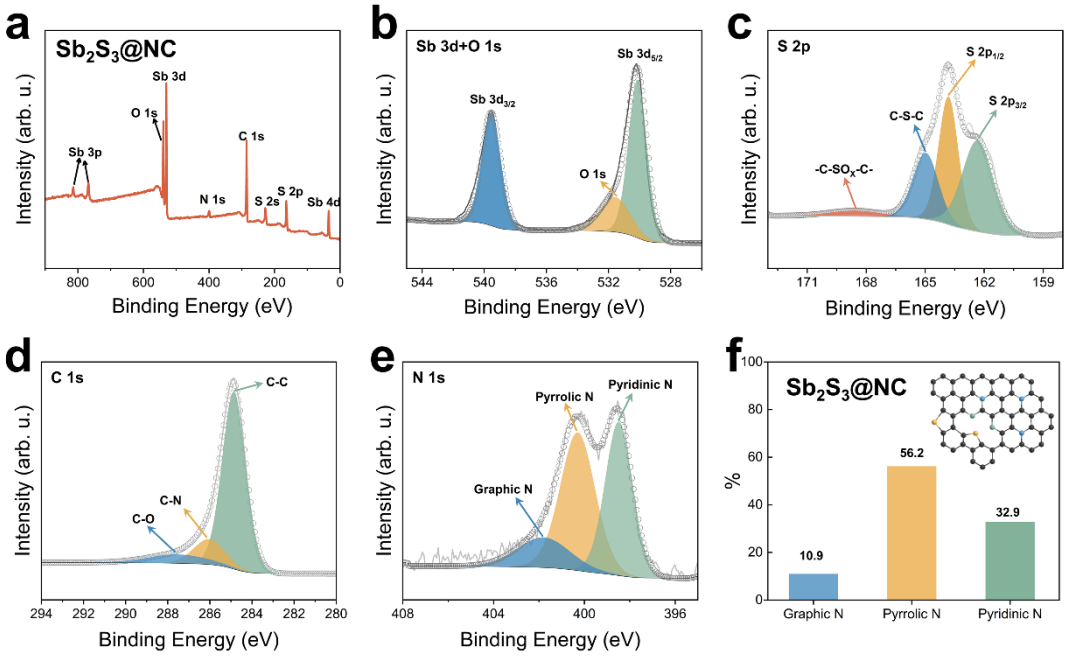

Fig.S9. (a) XPS survey spectrum and high-resolution XPS spectra of (b) Sb 3d/O 1s, (c) S 2p, (d) C 1s, and (e) N 1s of L-Sb_2S_3@NC; (f) Proportions of different types of nitrogen doping in Sb_2S_3@NC.

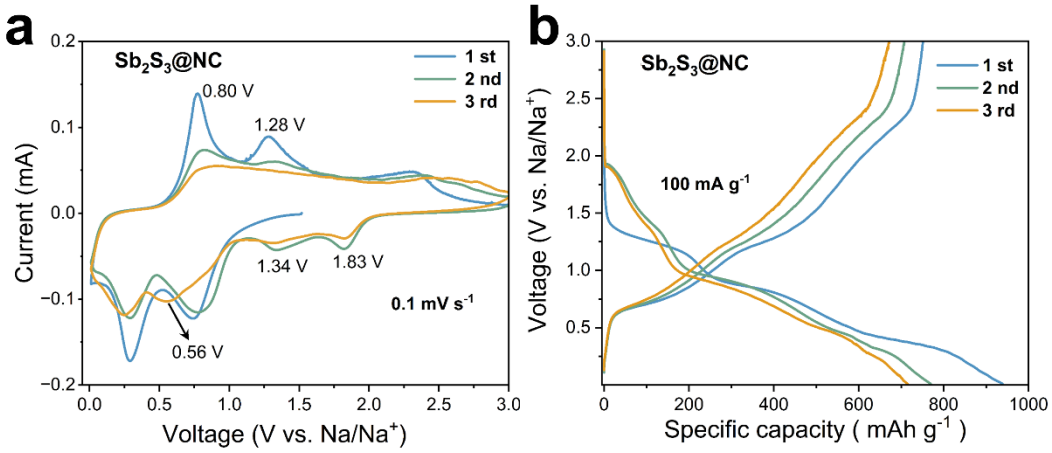

Fig.S10. (a) CV curves at 0.1 mV s^{-1} and (b) GCD profiles at 100 mA g^{-1} for first three cycles of Sb_2S_3@NC anode

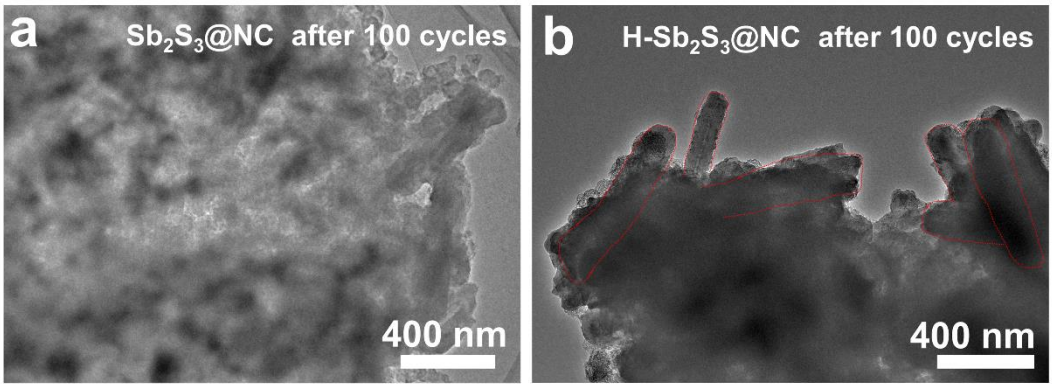

Fig.S11. TEM images of the Sb_2S_3@NC and H-Sb_2S_3@NC anodes after 100 cycles at 100 mA g^{-1}.

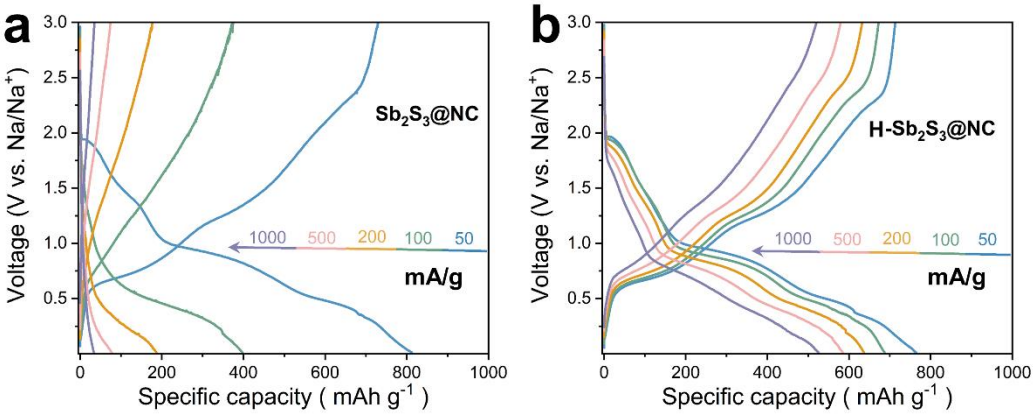

Fig.S12. GCD profiles of (a) Sb_2S_3@NC and (b) H-Sb_2S_3@NC anodes at various current corresponding to the rate capability as shown in Fig.4 (e).

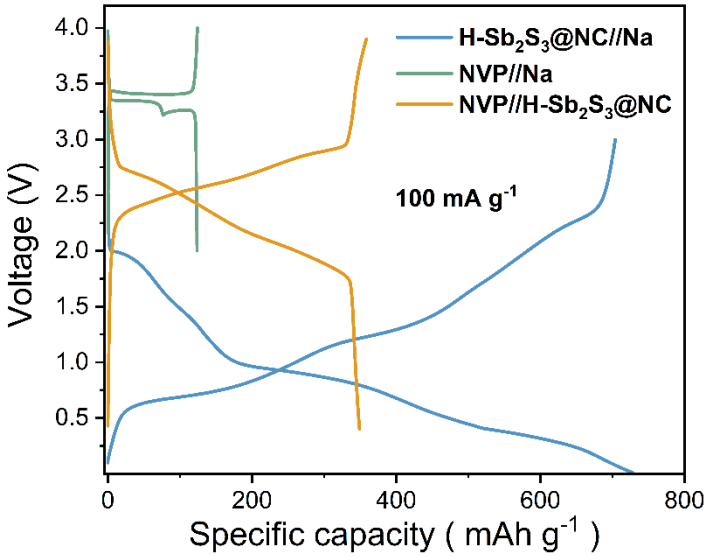

Fig.S13. GCD profiles of the pre-sodiated $Na_3V_2(PO_4)_3$ cathode and H-Sb_2S_3@NC anode.

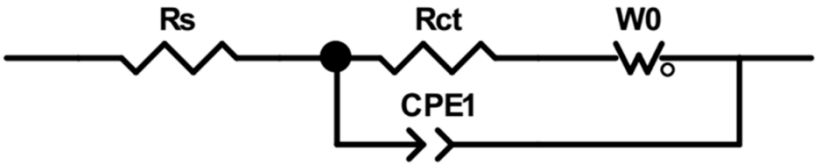

Fig.S14. Equivalent circuit model diagram.

Table S1. Electrolyte resistance (R_e) and charge transfer resistance (R_{ct}) of SIBs at different cycling states, fitted based on the same equivalent circuit。

Samples	States	R_e(Ω)	R_{ct}(Ω)
Sb_2S_3@NC	OCV	8.1	878.1
	After 30th cycles	15.1	5693.0
H-Sb_2S_3@NC	OCV	12.6	229.6
	After 30th cycles	4.9	159.8

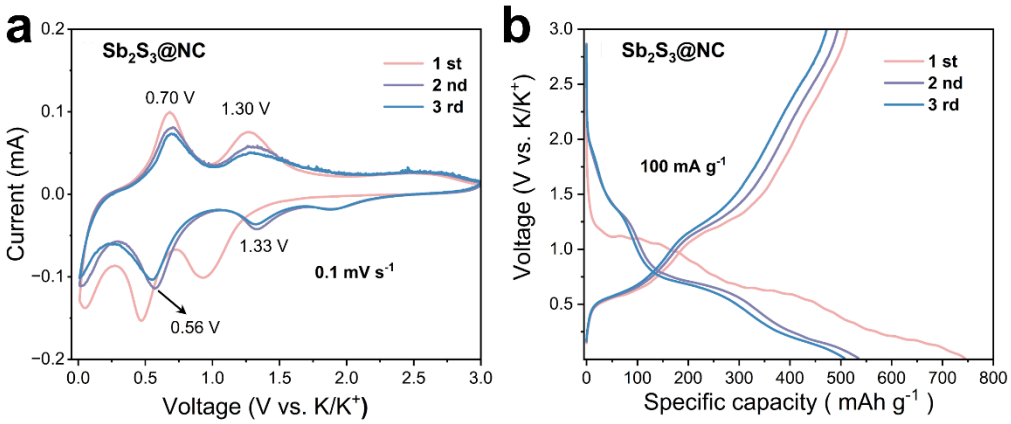

Fig.S15. (a) CV curves at 0.1 mV s^{-1} and (b) GCD profiles at 100 mA g^{-1} for first three cycles of Sb_2S_3@NC anode

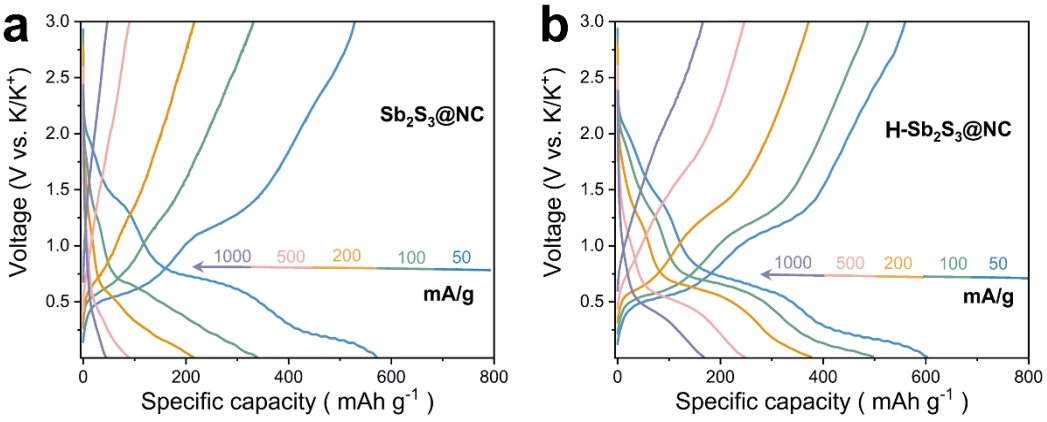

Fig.S16. GCD profiles of (a) Sb_2S_3@NC and (b) H-Sb_2S_3@NC anodes at various current corresponding to the rate capability as shown in Fig.7(d).

Table S2. Electrolyte resistance (R_e) and charge transfer resistance (R_{ct}) of PIBs at different cycling states, fitted based on the same equivalent circuit。

Samples	States	R_e(Ω)	R_{ct}(Ω)
Sb_2S_3@NC	OCV	12.7	5832.0
	After activation	18.2	2369.0
H-Sb_2S_3@NC	OCV	12.6	4894.0
	After activation	10.4	996.7